NASA Technical Memorandum 106122

A Modeling Investigation of Thermal and Strain Induced Recovery and Nonlinear Hardening in Potential Based Viscoplasticity

S.M. Arnold
Lewis Research Center
Cleveland, Ohio

A.F. Saleeb
University of Akron
Akron, Ohio

and

T.E. Wilt
University of Toledo
Toledo, Ohio

(NASA-TM-106122) A MODELING INVESTIGATION OF THERMAL AND STRAIN INDUCED RECOVERY AND NONLINEAR HARDENING IN POTENTIAL BASED VISCOPLASTICITY (NASA) 23 p

N94-11482

Unclas

G3/39 0176745

March 1993

NASA

A Modeling Investigation of Thermal and Strain Induced Recovery and Nonlinear Hardening in Potential Based Viscoplasticity

S. M. Arnold
National Aeronautics and Space Administration
Lewis Research Center
Cleveland OH, 44135

A. F. Saleeb
Department Civil Engineering
University of Akron
Akron, OH 44325

T. E. Wilt
NASA Resident Research Associate
University of Toledo
Toledo, OH 43606

Abstract

Specific forms for both the Gibb's and the complementary dissipation potentials were chosen such that a complete potential based multiaxial, isothermal, viscoplastic model was obtained. This model in general possesses three internal state variables (two scalars associated with dislocation density and one tensor associated with dislocation motion) both thermal and dynamic recovery mechanisms, and nonlinear kinematic hardening. This general model, although possessing associated flow and evolutionary laws, is shown to emulate three distinct classes of theories found in the literature, by modification of the driving threshold function F. A parametric study was performed on a specialized nondimensional multiaxial form containing only a single tensorial internal state variable (*i.e.*, internal stress). The study was conducted with the idea of examining the impact of including a strain-induced recovery mechanism and the *compliance operator*, derived from the Gibb's potential, on the uniaxial and multiaxial response. One important finding was that inclusion of strain-induced recovery provided the needed flexibility in modeling stress-strain and creep response of metals at low homologous temperatures, without adversely affecting the high temperature response. Furthermore, for nonproportional loading paths, the inclusion of the *compliance operator* had a significant influence on the multiaxial response, but had no influence on either uniaxial or proportional load histories.

1 Nomenclature

Invariants	
Ω	complementary dissipation potential
Φ	Gibb's complementary potential
F	Bingham-Prager threshold function
G, Ψ	normalized second invariant functions
J_2	second invariant of effective deviatoric stress tensor
I_2	second invariant of internal deviatoric stress tensor
H_1, H_2	invariant material functions
Stresses	
σ_{ij}	Cauchy stress tensor
S_{ij}	deviatoric stress tensor
Σ_{ij}	effective deviatoric stress tensor
α_γ	internal state variables (stress-like)
α_{ij}	internal (or back) stress tensor
a_{ij}	deviatoric internal stress tensor
κ, κ_o	drag stress and initial drag stress
Y	yield stress
Strains	
$e_{ij}, \epsilon^I_{ij}, \epsilon^R_{ij}, \epsilon^T_{ij}$	total, inelastic, reversable, and thermal strain tensors, resepectively
$\mathcal{A}_\gamma$	conjugate internal state variables (displacment-like)
$\mathcal{A}_{ij}$	internal strain tensor
$\mathcal{K}$	drag strain
$\mathcal{Y}$	yield strain
Material Parameters	
C_{ijkl}	elastic moduli tensor
H, R	hardening and thermal recovery material parameters
μ, B	material parameters
β	denotes the extent of strain induced recovery
n, m, p, q	material exponents
$g(G), f(F), x(\kappa), z(Y)$	material functions
$E(\sigma_{ij}), H(\alpha_\gamma), Z(T)$	material functions
η	coefficient of thermal expansion
Miscellaneous	
T, T_m, T_{melt}, T_o	applied, homologous, melting, and reference temperature, respectively.
t	real time
Υ	nondimensional time
$\mathcal{R}, \mathcal{B}$	nondimensional groups representing classes of materials
$Q1, Q2, Q3$	distinct compliance operators
δ_{ij}	Kroncker delta function
$\hat{\ }$	indicates variable normalized by initial drag stress, κ_o
$\langle\rangle$	Macauley Bracket
Hv[ ]	Heaviside unit function
$(\circ)$	nondimensional time derivative notation
$(\cdot)$	time derivative (or rate) notation

2 Introduction

In a previous publication [1], we reported on the general framework of viscoplastic representations based on the thermodynamics of irreversible processes and the internal variable formalism (for isotropic metals in the small-deformation regime under isothermal conditions). Emphasis in reference 1 was placed on the general forms and broad restrictions imposed in the context of a *complete* (i.e., fully associative) potential structure. In particular, in this formulation there are two key ingredients: (1) the thermodynamic potential, or Gibbs function, defining the equations of state, and (2) the viscoplastic dissipation function for the ensuing flow and evolution laws, of inelastic strain and internal state parameters, respectively.

In order to progress further, one has to model the specific features of the material concerned (*e.g.*, take into consideration experimental observations and also, whenever possible the physics of the phenomena involved). This then calls for (1) introducing specialized forms, in terms of the state and internal-parameter sets selected, of the potential functions mentioned previously and (2) a careful investigation of the impact of these forms on the characteristics of the resulting constitutive model. A detailed study involving these two points is the main focus of the present paper. To this end, we shall consider a fairly-comprehensive set of equations that are developed here as a subclass of what we, in reference 1, termed the decoupled-form, that is, a form encompassing such important features as nonlinear-kinematic hardening and both dynamic (strain) and static (thermal) recovery effects. For convenience, we shall make use of a nondimensional format of a specific model and construct the plots of the associated state space [2,3] to gain further insight into the consequences of the parameters and functional forms chosen with regard to the model's predictive capabilities.

Although several quantitative results and comparisons are given, we still emphasize that the proposed equations by no means suggest a specific model intended for immediate utilization. This is particularly true with regard to the cyclic response that was modeled (especially in the presence of nonlinear-kinematic hardening) where measures such as irreversibility constraints, loading-unloading conditions, limit-surface concepts, and so on are often utilized to prevent abnormalities in the predicted stress-strain curves upon unloading and reversed loading. We have introduced such internal state discontinuity inequalities in the present model by following approaches currently in common use [*e.g.* 4-6]. However, more work is certainly needed for a valid assessment of such an adhoc treatment, especially in the present context of potential-based forms, where the associativeness of the evolutionary equations is compromised. Finally, in view of the results obtained here, we firmly believe that the present forms provide several important ingredients needed in developing successful models for specific materials. In fact, this work is currently underway, and the results for characterization of models of this type will be reported subsequently.

3 Complete Potential Structure

Here the basic thermodynamic framework put forth by Arnold and Saleeb [1] is summarized. Expressions for the Gibb's thermodynamic and the complementary dissipation potential functions, in terms of a number of state and internal variables characterizing the changing internal structure of the material, are assumed. For conciseness, the discussion is limited to a case involving small deformations (in which the initial state is assumed to be stress free throughout), an initially isotropic material, isothermal conditions and the decoupled potential framework [1]. A Cartesian coordinate reference frame and index notation are utilized (repeated Roman subscripts imply summation).

Given the Gibb's potential in the following form

$$\Phi = \Phi(\sigma_{ij}, \alpha_\gamma, T, \epsilon^I_{ij}) \tag{1}$$

and assuming *a priori* that the inelastic strain is an independent parameter (and not an internal state variable) for example,

$$\Phi = E(\sigma_{ij}) - \sigma_{ij}\epsilon^I_{ij} + \bar{H}\,(\alpha_\gamma) - Z(T) - \frac{\sigma_{kk}}{3}\eta(T - T_o) \tag{2}$$

an expression for the total strain rate can be obtained by differentiating:

$$\dot{e}_{ij} = \frac{d}{dt}\left(\frac{-\partial\Phi}{\partial\sigma_{ij}}\right) = \frac{-\partial^2\Phi}{\partial\sigma_{ij}\partial\sigma_{rs}}\dot{\sigma}_{rs} + \dot{\epsilon}^I_{ij} + \delta_{ij}\frac{\eta}{3}\dot{T} \tag{3}$$

The three terms in equation (3) may then be identified as the reversible, irreversible (inelastic), and thermal expansion components of the total strain rate, respectively. Thus,

$$\dot{e}_{ij} = \dot{\epsilon}^R_{ij} + \dot{\epsilon}^I_{ij} + \dot{\epsilon}^T_{ij} \tag{4}$$

where

$$\dot{\epsilon}^R_{ij} = \frac{-\partial^2\Phi}{\partial\sigma_{ij}\partial\sigma_{rs}}\dot{\sigma}_{rs} \tag{5}$$

and

$$\dot{\epsilon}^T_{ij} = \delta_{ij}\frac{\eta}{3}\dot{T} \tag{6}$$

but $\dot{\epsilon}^I_{ij}$ (the inelastic strain rate) is defined separately by using the concept of a dissipation potential $\Omega(\sigma_{ij}, \alpha_\gamma, T)$.

Given

$$\Omega = \Omega(\sigma_{ij}, \alpha_\gamma, T) \tag{7}$$

then by using the Clausius-Duhem inequality, the flow law can be written as

$$\dot{\epsilon}^I_{ij} = \frac{\partial\Omega}{\partial\sigma_{ij}} \tag{8}$$

the evolutionary laws for the thermodynamic conjugate internal state variables written as

$$\dot{A}_\gamma = -\frac{\partial\Omega}{\partial\alpha_\gamma} \tag{9}$$

and the constitutive equations for the rate of internal state variables as,

$$\dot{\alpha}_\gamma = [Q_{\gamma\ell}]^{-1}\,\dot{A}_\ell \tag{10}$$

where

$$Q_{\gamma\ell} = \frac{-\partial^2\,\bar{H}}{\partial\alpha_\gamma\partial\alpha_\ell} \tag{11}$$

Thus equations (8), and (9) represent the flow and evolutionary laws, for an assumed $\Omega = \Omega(\sigma_{ij}, \alpha_\gamma, T)$ and equation (10) the internal constitutive rate equations, given a Gibb's potential Φ, wherein both potentials are directly linked through the internal state variables α_γ.

4 Elastic/Viscoplastic Constitutive Model

A complete multiaxial statement can be derived by using the above framework, given a specific form for both the Gibb's potential, Φ, and the complementary dissipation potential, Ω. Form invariance (objectivity) of these potentials requires that they depend only on certain invariants of their respective tensorial arguments (*i.e.*, an integrity basis [7]). In the spirit of von Mises and because of the deviatoric nature of inelastic deformation, only the quadratic invariant will be considered at this time in specifying the dissipation potential. Similarly, only the linear elastic strain energy contribution will be considered in specifying the Gibb's potential, with the internal state groupings being functions of the respective quadratic invariants. Finally, although equation (7) indicates that an unlimited number of internal state variables can be specified, here our attention will be restricted to a constitutive model with, at most, three internal state variables. The first internal state variable, a_{ij}, is taken to be a second order symmetric traceless tensor that represents the internal (or back) stress associated with dislocation motion. The second and third internal variables (κ and Y) are scalar state variables representing the drag and yield stresses, respectively, which are associated with dislocation density.

Consequently, the Gibb's potential may be written as

$$\Phi = -\frac{1}{2}C_{rskl}\sigma_{rs}\sigma_{kl} - \sigma_{ij}\epsilon^I_{ij} + H_1(G) + H_2(\Psi) - Z(T) - \frac{\sigma_{kk}}{3}\eta(T - T_o) \tag{12}$$

and the dissipation potential as

$$\Omega = \mu \int f(F)dF + \frac{R\mu}{H}\int g(G)dG + \int x(\kappa)d\kappa + \frac{1}{B}\int z(Y)dY \tag{13}$$

where

$$F = \left\langle \frac{J_2}{\kappa^2} + \beta G - \Psi^2 \right\rangle \tag{14}$$

$$G = \frac{I_2}{\kappa^2} \tag{15}$$

$$\Psi = \frac{Y}{\kappa} \tag{16}$$

$$H_1(G) = \frac{\mu}{H}G^{p+1} \tag{17}$$

$$H_2(\Psi) = \frac{1}{B}\Psi^q \tag{18}$$

$$I_2 = \frac{3}{2}a_{ij}a_{ij} \tag{19}$$

$$J_2 = \frac{3}{2}\Sigma_{ij}\Sigma_{ij} \tag{20}$$

$$\Sigma_{ij} = S_{ij} - a_{ij} \tag{21}$$

$$S_{ij} = \sigma_{ij} - \frac{1}{3}\sigma_{kk}\delta_{ij} \tag{22}$$

$$a_{ij} = \alpha_{ij} - \frac{1}{3}\alpha_{kk}\delta_{ij} \tag{23}$$

Note that in the preceding expression for the dissipation potential, the stress dependence, both external and internal, enters through the scalar functions F and G in the form of effective (Σ_{ij}) and

internal (a_{ij}) deviatoric stresses, respectively. Furthermore, the function F acts like a threshold surface, because when $F < 0$, no inelastic strain can occur. Note that the function F was chosen in such a way that it would emulate the features of three types (or classes) of viscoplastic theories commonly found in the literature. The first class is composed of the models without a yield (or threshold) surface, that is, those in which $Y = 0$ (*i.e.*, $\Psi = 0$), which includes models proposed by Miller[8], Walker[9], Krempl et al.[10], and others. The second are those with no evolving drag strength (*i.e.*, $\kappa = constant$), yet which have a threshold surface, as used by Chaboche[11], Freed and Walker[12], and others; and the third class are those theories with a threshold surface but wherein both the yield and drag stresses are proportional, (*i.e.*, $Y \propto \kappa$) as put forth by Perzyna[13], Robinson[5,14] and others.

By selecting the preceding scalar functions, a general yet *complete* potential-based model, with *associated* flow and evolutionary laws that will encompass a wide range of the models found in the literature can be constructed. The second invariants , J_2 and I_2 , are also scaled for tension. These invariants could just as easily have been scaled for shear by replacing the coefficient 3/2 with 1/2, and modifying the definition of the magnitude of the inelastic strain rate that follows. Also, by including an additional term, βG, which is a scaled function of the internal deviatoric stress and drag stress, allows for the presence of a strain induced recovery term in the evolution of the associated conjugate variable ($\mathcal{A}_{kl}$), as discussed later. It is interesting to note the close similarity between the present assumed form of the threshold surface F of equation (14) to that used by Lemaitre and Chaboche [15] in the context of inviscid plasticity. The significant difference between the two forms is that Lemaitre and Chaboche [15] utilized a non-associated format; the form similar to equation (14) was taken to affect only the directions of inelastic and internal state whereas a classical J_2 form was employed to control yielding (*i.e.*, the consistency condition). In the present fully associative case, the same threshold surface F is used to affect both yielding,, and the direction of inelastic and internal state.

Taking the appropriate derivatives of both Φ and Ω as indicated in equations (2) through (12), one obtains the multiaxial isothermal specification particular to the present constitutive model. Here the decomposition of the total strain rate is that of equation (4), where the reversible strain rate is,

$$\dot{\epsilon}^R_{ij} = C_{ijkl}\dot{\sigma}_{kl} \tag{24}$$

and the irreversible (or inelastic) strain rate is defined as

$$\dot{\epsilon}^I_{ij} = \frac{3}{2}\|\dot{\epsilon}^I_{ij}\|\frac{\Sigma_{ij}}{\sqrt{J_2}} \tag{25}$$

where

$$\|\dot{\epsilon}^I_{ij}\| = \sqrt{\frac{2}{3}\dot{\epsilon}^I_{ij}\dot{\epsilon}^I_{ij}} = \frac{2\mu f(F)}{\kappa^2}\sqrt{J_2} \tag{26}$$

and the internal state variable constitutive laws relating the associated rates of the thermodynamic variables and their respective conjugates are

$$\dot{a}_{ij} = [Q1_{ijkl}]^{-1}\,\dot{\mathcal{A}}_{kl} \tag{27}$$

$$\dot{\kappa} = Q2^{-1}\dot{\mathcal{K}} \tag{28}$$

$$\dot{Y} = Q3^{-1}\dot{\mathcal{Y}} \tag{29}$$

with Q1, Q2, and Q3 being distinctly different operators.

The evolutionary laws for the thermodynamic conjugate variables are then obtained from equation (9):

$$\dot{\mathcal{A}}_{kl} = \dot{\epsilon}^I_{kl} - \frac{3}{2}\frac{\beta}{\sqrt{J_2}}||\dot{\epsilon}^I_{ij}||a_{kl} - \frac{3R\mu\, g(G)}{H\kappa^2}a_{kl} \tag{30}$$

$$\dot{\mathcal{K}} = \frac{1}{\kappa}\{S_{ij}\dot{\epsilon}^I_{ij} - a_{ij}\dot{\mathcal{A}}_{ij} - Y\,\dot{\mathcal{Y}}\} - \frac{z(Y)Y}{B\kappa} - x(\kappa) \tag{31}$$

$$\dot{\mathcal{Y}} = \frac{Y}{\sqrt{J_2}}||\dot{\epsilon}^I_{ij}|| - \frac{z(Y)}{B} \tag{32}$$

And the respective *compliance operators* from equation (11) are

$$Q1_{ijkl} = \frac{3\mu(p+1)}{H\,\kappa^2}G^p[\frac{3p}{\kappa^2 G}\,a_{kl}a_{ij} + I_{ijkl}] \tag{33}$$

$$Q2 = \frac{2\mu(p+1)}{H\,\kappa^2}(2p+3)G^{p+1} + \frac{q(q+1)}{\kappa^2}(\Psi)^q \tag{34}$$

$$Q3 = \frac{q(q-1)}{B\,\kappa^2}(\Psi)^{q-2} \tag{35}$$

with $I_{ijkl} = \delta_{ik}\delta_{jl}$. Finally, inversion of the compliance operators results in

$$[Q1_{ijkl}]^{-1} = \frac{\kappa^2 H}{3\mu(p+1)G^p}[I_{ijkl} - \frac{3p}{\kappa^2(2p+1)G}a_{kl}a_{ij}] \tag{36}$$

$$Q2^{-1} = \frac{HB\kappa^2}{2B\mu(p+1)(2p+3)G^{p+1} + q(q+1)H\Psi^q} \tag{37}$$

$$Q3^{-1} = \frac{B\kappa^2}{q(q-1)}\Psi^{2-q} \tag{38}$$

An examination of the evolution of the conjugate of the internal stress (*i.e.*, the internal strain, $\mathcal{A}_{ij}$), clearly shows that equation (30) possesses, as typically assumed in the literature [16,17], a competitive process of a hardening term (which accounts for strengthening mechanisms) and two recovery terms (which account for softening mechanisms). The first recovery term evolves with plasticity; it is strain induced, and is commonly called dynamic recovery. The second term, interchangeably called static or thermal recovery, evolves with time and is thermally induced.

The evolution of the conjugate of the drag stress (*i.e.*, the internal drag strain, $\mathcal{K}$), equation (31), is driven by three energy sources. The first is the dissipated plastic work ($S_{ij}\dot{\epsilon}^I_{ij}$), and the second and third, respectively, are the energy changes due to internal structure (dislocation) rearrangement ($a_{ij}\dot{\mathcal{A}}_{ij}$) and the yield related dislocation density contribution ($Y\,\dot{\mathcal{Y}}$). The static recovery terms ($z(Y)$ and $x(\kappa)$) also evolve with time and are thermally induced. Finally, from equation (32) one can see that a scaled plastic strain ($||\dot{\epsilon}^I_{ij}||$) is driving the evolution of the conjugate of the yield stress (*i.e.*, the internal yield strain, $\mathcal{Y}$) and is in direct competition with a thermal recovery term $z(Y)$.

4.1 Specializations

The preceding model, which consists of three internal state variables, can be specialized into the three classes of viscoplastic models discussed previously. Note that in all specializations the form of the inelastic strain rate does not change, only its functional dependence on F. Similarly, the applicable internal rate constitutive laws (eqs. (27) to (29)) remain unchanged as well.

Consider the first class of models, those models without a threshold surface (*i.e.*, no yield stress; $Y = 0$). Here

$$F = \left\langle \frac{J_2}{\kappa^2} + \beta G \right\rangle \tag{39}$$

and the associated evolutionary laws are equations (30) and

$$\dot{\mathcal{K}} = \frac{1}{\kappa}\{S_{ij}\dot{\epsilon}^I_{ij} - a_{ij}\,\dot{\mathcal{A}}_{ij}\} - x(\kappa) \tag{40}$$

which can also be rewritten as

$$\dot{\mathcal{K}} = \frac{1}{\kappa}\left\{\Sigma_{ij}\dot{\epsilon}^I_{ij} + \frac{\beta}{\sqrt{J_2}}||\dot{\epsilon}^I_{ij}||I_2 + \frac{2R\mu g(G)}{H}G\right\} - x(\kappa) \tag{41}$$

The second class of models, those containing a threshold surface wherein the drag stress is held constant ($\kappa = \kappa_o$), is obtained by assuming

$$F = \left\langle \frac{J_2 + \beta I_2}{\kappa_o^2} - \frac{Y^2}{\kappa_o^2} \right\rangle \tag{42}$$

with the associated evolutionary laws given by equations (30) and (32). If we further specialize this model to one that has only a single scalar, internal state variable, Y (by eliminating the internal deviatoric stress; i.e., $I_2 = 0$), equation (42) becomes

$$F = \left\langle \frac{J_2 - Y^2}{\kappa_o^2} \right\rangle \tag{43}$$

and equation (32) is modified to become

$$\dot{\mathcal{Y}} = \frac{Y}{\sqrt{J_2}}||\dot{\epsilon}^I_{ij}|| - \frac{z(Y)}{B} \tag{44}$$

with $J_2 = \frac{3}{2}S_{ij}S_{ij}$. Equations (43) and (44) are then similar to other yield strength models found in the literature, the only difference being the scaling parameter in the hardening term and the presence of the compliance operator $Q3$ in the internal variable constitutive law of equation (29).

Finally, the third class of models, those models that possess a threshold surface but which assume that both the yield and drag stress are proportional ($Y \propto \kappa$), can be represented by

$$F = \left\langle \frac{J_2}{\kappa^2} + \beta G - 1 \right\rangle \tag{45}$$

with the associated evolutionary laws given by equations (30) and (40).

Here, the specific form to be investigated will be an internal (or back) stress model of the third class ($Y = \kappa = \kappa_o$); that is,

$$F = \left\langle \frac{J_2 + \beta I_2}{\kappa_o^2} - 1 \right\rangle \tag{46}$$

with the flow law given by equations (25) and (26) and the internal constitutive law and the evolutionary law given by equations (27), (30) and (36). This model, hencforth, will be called the modified model, since it is the corrected form of the Robinson model [4,14] as discussed in reference 1, with an additional strain-induced recovery term introduced by including the βI_2 term in the threshold function F. The primary objectives of this study are to illustrate the effect of the compliance operator ($Q1_{ijkl}$) and to examine the importance of including a strain-induced (dynamic) recovery term, under both multiaxial and uniaxial states of stress, with the limitations imposed by considering only a single tensorial internal state variable. This will be accomplished by mapping out the associated state space and the stress-strain response.

5 Nondimensional Multiaxial Form

For generality and computational convenience, let us nondimensionalize the specific model to be examined by using the following dimensionless variables and parameter groups. Normalizing the applied and internal stress components relative to the initial drag strength κ_o of the given material gives the dimensionless stresses

$$\hat{\sigma}_{ij} = \frac{\sigma_{ij}}{\kappa_o} \tag{47}$$

and

$$\hat{\alpha}_{ij} = \frac{\alpha_{ij}}{\kappa_o} \tag{48}$$

The time is nondimensionlized relative to the hardening material parameter H, which is defined in units per time, by multiplying by the real time t. Thus,

$$\Upsilon = H\ t \tag{49}$$

where Υ is the nondimensional time. As a consequence of equation (49), the rate of change of real and nondimensional time are related by

$$\frac{d}{d\Upsilon} = \frac{1}{H}\frac{d}{dt} \tag{50}$$

Henceforth $d/d\Upsilon$ will be denoted by an open circle appearing over a quantity, that is, $(\circ)$. Two dimensionless parameter groups are taken as

$$\mathcal{R} = \frac{R}{H} \tag{51}$$

and

$$\mathcal{B} = \frac{\mu}{H\kappa_o} \tag{52}$$

where $\mathcal{R}$ is a measure of the relative importance of the thermal recovery and hardening terms (R and H) which appear in the evolutionary equation. Similarly, $\mathcal{B}$ may be considered a measure of the relative importance of *viscous dissipation* to *plastic dissipation*. As pointed out by Robinson [14], $\mathcal{B}$ is related to the reciprocal of the Bingham number as defined by Prager [18].

Given the preceding relations, the nondimensional multiaxial representation of equations (27), (30), (36), and (46) can be written as

$$\overset{\circ}{\epsilon}{}^{I}_{ij} = \frac{3}{2}||\dot{\epsilon}^{I}_{ij}||\frac{\hat{\Sigma}_{ij}}{\sqrt{\hat{J}_2}} \qquad \text{if} \quad \hat{\Sigma}_{ij}\hat{a}_{ij} > 0 \tag{53}$$

$$\overset{\circ}{\epsilon}{}^{I}_{ij} = 0 \qquad \text{if} \quad \hat{\Sigma}_{ij}\hat{a}_{ij} \leq 0$$

$$|| \overset{\circ}{\epsilon}{}^{I}_{ij} || = \sqrt{\frac{2}{3}\overset{\circ}{\epsilon}{}^{I}_{ij}\overset{\circ}{\epsilon}{}^{I}_{ij}} = 2\mathcal{B}f(\hat{F})\sqrt{\hat{J}_2} \tag{54}$$

and

$$\overset{\circ}{\hat{a}}_{ij} = [\hat{Q}1_{ijkl}]^{-1}\ \overset{\circ}{\mathcal{A}}_{kl} \tag{55}$$

$$\overset{\circ}{\mathcal{A}}_{kl} = \overset{\circ}{\epsilon}{}^{I}_{kl} - \frac{3}{2}\frac{\beta}{\sqrt{\hat{J}_2}}|| \overset{\circ}{\epsilon}{}^{I}_{ij} ||\hat{a}_{kl} - 3\mathcal{R}\mathcal{B}g(\hat{\aleph})\hat{a}_{kl} \tag{56}$$

where

$$[\hat{Q}1_{ijkl}]^{-1} = \frac{1}{3B(p+1)\hat{\aleph}^p}[I_{ijkl} - \frac{3p}{(2p+1)\hat{G}}\,\hat{a}_{kl}\hat{a}_{ij}] \tag{57}$$

and

$$\hat{F} = \hat{J}_2 + \beta\hat{G} - 1 \tag{58}$$

$$\hat{G} = \hat{I}_2 \tag{59}$$

$$\hat{I}_2 = \frac{3}{2}\hat{a}_{ij}\hat{a}_{ij} \tag{60}$$

$$\hat{J}_2 = \frac{3}{2}\hat{\Sigma}_{ij}\hat{\Sigma}_{ij} \tag{61}$$

$$\hat{\Sigma}_{ij} = \hat{S}_{ij} - \hat{a}_{ij} \tag{62}$$

$$\hat{\aleph} = \langle \hat{G} - \hat{G}_o \rangle \mathrm{Hv}[\hat{S}_{ij}\hat{a}_{ij}] + \hat{G}_o \tag{63}$$

Now further specializing the above expressions by assuming nonlinearity of the inelasticity and expressing the thermal recovery dependence by a power law function, we assume

$$f(\hat{F}) = \left\langle \hat{F} \right\rangle^n \tag{64}$$

and

$$g(\hat{\aleph}) = \hat{\aleph}^m \tag{65}$$

In the preceding expressions, <>represents the Macauley bracket operator and Hv[ ] denotes the Heaviside unit function.

Furthermore, we impose the internal state discontinuity regions suggested by Robinson [5,14]. These regions are implied by the resetting of $\hat{G}$ to an initial value $\hat{G}_o$ whenever the product $\hat{S}_{ij}\hat{a}_{ij}$ becomes negative in $\hat{\aleph}$, equation (63). The creation of these regions is motivated by the essential need to capture the cyclic response indicated experimentally within the framework of nonlinear kinematic hardening. We emphasize that this is an adhoc treatment in the present context; however, this inconsistency relative to the potential structure becomes irrelevant for all of the monotonic-load applications considered in the subsequent sections. Hence all conclusions reached remain valid.

5.1 Uniaxial Simplification and State Space Representation

If we consider only a uniaxial state of stress, the dimensionless deviatoric applied and internal stress tensors become

$$\hat{S}_{ij} = \frac{1}{3}\begin{bmatrix} 2\hat{\sigma} & 0 & 0 \\ 0 & -\hat{\sigma} & 0 \\ 0 & 0 & -\hat{\sigma} \end{bmatrix}$$

and

$$\hat{a}_{ij} = \frac{1}{3}\begin{bmatrix} 2\hat{\alpha} & 0 & 0 \\ 0 & -\hat{\alpha} & 0 \\ 0 & 0 & -\hat{\alpha} \end{bmatrix}$$

such that

$$\hat{F} = (\hat{\sigma} - \hat{\alpha})^2 + \beta\hat{\alpha}^2 - 1$$

$$\hat{G} = \hat{\alpha}^2$$

and the flow and evolutionary laws, respectively, become

$$\overset{\circ}{\epsilon}{}^{I} = 2\mathcal{B}\langle\hat{F}\rangle^n(\hat{\sigma} - \hat{\alpha}) \tag{66}$$

and

$$\overset{\circ}{\hat{\alpha}} = \frac{1}{2\mathcal{B}(p+1)(2p+1)}\left\{1 - \frac{\beta\hat{\alpha}}{(\hat{\sigma} - \hat{\alpha})}\right\}\frac{\overset{\circ}{\epsilon}{}^{I}}{\hat{\aleph}^p} - \frac{\mathcal{R}}{(p+1)(2p+1)}\hat{\aleph}^{(m-p)}\hat{\alpha} \tag{67}$$

Utilizing the concept of the state space representation [2,3,19], we can examine and illustrate geometrically the various features of the present unified viscoplastic model, in particular the effect of the strain-induced recovery term. The pertinent state spaces are constructed by combining and rewriting equations (4), (24), (66), and (67), in standard vector form as follows, and plotting the corresponding $\mathcal{G}$ fields or relaxation trajectories. That is,

$$\overset{\circ}{\mathcal{S}} = \mathcal{G}(\hat{\sigma}, \hat{\alpha}) + \overset{\circ}{\mathcal{D}}(\overset{\circ}{e})$$

or

$$\begin{Bmatrix} \overset{\circ}{\hat{\sigma}} \\ \overset{\circ}{\hat{\alpha}} \end{Bmatrix} = \begin{Bmatrix} -\hat{E}\,\overset{\circ}{\epsilon}{}^{I} \\ \frac{\hat{H}}{\hat{\aleph}^p}\{1 - \frac{\beta\hat{\alpha}}{\hat{\sigma} - \hat{\alpha}}\}\,\overset{\circ}{\epsilon}{}^{I} - \hat{R}\hat{\aleph}^{(m-p)}\hat{\alpha} \end{Bmatrix} + \begin{Bmatrix} \hat{E}\,\overset{\circ}{e} \\ 0 \end{Bmatrix} \tag{68}$$

where

$$\hat{E} = \frac{E}{\kappa_o}$$

$$\hat{H} = \frac{1.0}{2\mathcal{B}(p+1)(2p+1)}$$

$$\hat{R} = \frac{\mathcal{R}}{(p+1)(2p+1)}$$

$$\hat{\aleph} = \langle\hat{\alpha}^2 - \hat{\alpha}_o^2\rangle \mathrm{Hv}[\frac{4}{9}\hat{\sigma}\hat{\alpha}] + \hat{\alpha}_o^2$$

and $\overset{\circ}{e}$ is the nondimensional total uniaxial strain rate. These relaxation trajectories are obtained from equations (66) and (68) by imposing (1) a constant nondimensional total strain rate (*i.e.*, $\overset{\circ}{e} = 0$), thereby implying that $\overset{\circ}{\mathcal{S}} = \mathcal{G}(\hat{\sigma}, \hat{\alpha})$, and (2) a set of baseline material parameters as follows:

$$\begin{gathered} \kappa = 0.5774 \\ \mu = 1.39\text{x}10^{-9} \\ H = 3.55\text{x}10^{-4} \\ R = 3.74\text{x}10^{-3} \\ n = 4 \\ p = 0.575 \\ m = 4.365 \end{gathered}$$

5.1.1 Dynamic and Thermal Recovery Effects

Figures 1 to 6 illustrate the state space representation associated with equations (66), (68), and the base-line material parameters given previously, for three values of β and two values of $\mathcal{R}$. These are, respectively; $\mathcal{R} = 10.535$ with $\beta = 0$, 0.5, and 1.0; and $\mathcal{R} = 0$ with $\beta = 0, 0.5$ and 1.0. Note that $\mathcal{R} = 0$ can be associated with low homologous temperatures ($T_m = T/T_{melt} < 0.2$), whereas $\mathcal{R} = 10.535$ can be associated with some elevated temperature (*e.g.*, $T_m > 0.35$) at which thermally activated mechanisms exist.

Immediately a number of qualitative features of the first quadrant of the state space can be deduced from equations (66) and (68). For example, the locus of steady state (or *fixed*) points in creep, denoted by line *ab* in Figs. 1 to 6, is obtained by imposing the condition $\overset{\circ}{\mathcal{S}} = 0$ on equations (68). Mathematically, such a condition is obtained when

$$\hat{\sigma} = \hat{\alpha} + \left[1 - \beta\hat{\alpha}^2 + \left\{\hat{R}\frac{\hat{\alpha}^{2m+1}}{[\hat{\sigma} - (1+\beta)\hat{\alpha}]}\right\}^{1/n}\right]^{1/2} \tag{69}$$

and is denoted as the locus of steady state creep, see line *ab*. The associated steady state creep rate is

$$\overset{\circ}{\epsilon}^I = \frac{\hat{R}}{\hat{H}}\frac{\hat{\alpha}^{2m+1}}{\left(1 - \frac{\beta\hat{\alpha}}{\hat{\sigma}-\hat{\alpha}}\right)} \tag{70}$$

Secondly, the locus of maxima in stress (*i.e.*, $\overset{\circ}{\hat{\sigma}} = 0$) during relaxation ($\overset{\circ}{e} = 0$) occurs when

$$\overset{\circ}{\epsilon}^I = -\frac{\overset{\circ}{\hat{\sigma}}}{\hat{E}} = 0 \tag{71}$$

or when

$$\hat{F}^n(\hat{\sigma} - \hat{\alpha}) = 0 \tag{72}$$

This is satisfied when either

$$\hat{\sigma} = \hat{\alpha} \tag{73}$$

(denoted by line *de* in Figs. 1 to 6) or

$$\hat{\sigma} = \hat{\alpha} + (1 - \beta\hat{\alpha}^2)^{1/2} \tag{74}$$

(denoted by line *ac* in Figs. 1 to 6). The points on lines *ac* and *de* do not correspond to fixed points in the state space, as do those associated with line *ab*, since the internal stress continues to evolve, that is,

$$\overset{\circ}{\hat{\alpha}} = -\hat{R}\,\hat{\alpha}^{2(m-p)+1} \tag{75}$$

Note that the inelastic strain rate is zero in this region of the state space as a result of invoking the load-unload inequalities in equation (53). Clearly this continued evolution occurs only if the temperature is sufficiently high to induce thermal recovery (*i.e.*, $\mathcal{R} \neq 0$), as in Figs. 1 to 3. For example, when the homologous temperature is low (*i.e.* , $T_m < 0.2$, room temperature for most superalloys), $\mathcal{R} = 0$ and the locus of maxima in stress (lines *ac* and *de*) will become *fixed* points (see Figs. 4 to 6).

Furthermore, comparing the elevated temperature behavior (Figs. 1 to 3) to the low temperature behavior (Figs. 4 to 6), we make the following observations. First, with no strain-induced recovery (*i.e.*, $\beta = 0$),the model will predict a purely nonlinear hardening response with no secondary creep regime and no internal recovery occurring below the line *ac*, (see Fig. 4). Alternatively, at elevated temperature both secondary creep and internal recovery are predicted. Second, when strain-induced recovery is present

(*i.e.*, $\beta \neq 0$) and T_m is still low ($\mathcal{R} = 0$), secondary creep can occur. However, no internal recovery will take place below the line *acde*, owing to the inclusion of the inequalities on $\overset{\circ}{\epsilon}^I$. Also, observe that for $\mathcal{R} = 0$ the locus of steady state is linear, whereas for $\mathcal{R} \neq 0$ it is a nonlinear function of internal stress ($\hat{\alpha}$) (see line *ab* in Figs. 1 to 6).

Using the evolutionary law in equations (68) and considering a case wherein strain-induced recovery is removed ($\beta = 0$), we can show (see Fig. 7) the effect of increasing the thermal recovery term $\mathcal{R}$ (*i.e.*, increasing the temperature) on the relaxation trajectory labeled *fa* in Fig. 1. Note that $\mathcal{R}$ has no effect on the initial relaxation rate, but rather moves the location of the stationary point (steady state creep) up and to the left as indicated by the movement of point *g*. Furthermore, if $\mathcal{R} = 0$, *g* becomes not only a fixed point in creep, but one in relaxation as well. Also for any nonzero $\mathcal{R}$ value we see that the internal stress can, given sufficient time, return to zero, whereas the stress supported by the material will return to the initial threshold stress κ_o.

Assuming the presence of strain induced recovery mechanisms (*i.e.*, $\beta \neq 0$, see Fig. 8), we see that even when thermal recovery is not present (*i.e.*, $\mathcal{R} = 0$) a stationary point in creep will now exist (see point *g* in Fig. 8). Also the line *ac* and *de* of fixed points in relaxation become curved and shifted, respectively, as compared to Fig. 7. As in figure 7, again we see that including β and varying $\mathcal{R}$ does not affect the initial relaxation rates (path *f* to *g*) until, the point *g* associated with steady state creep is approached and traversed. The initial relaxation rate is, however, greatly affected by changes in the nondimensional parameter $\mathcal{B}$ as clearly shown in Fig. 9 where $\mathcal{B}$ is varied by two orders of magnitude while β and $\mathcal{R}$ are held fixed at 0 and 10.535, respectively. Note that because of this change in initial hardening, the location of steady state moves along the locus specified by equation (69) since the applied and internal stress reached increases with increasing values of $\mathcal{B}$.

In summary, from the viewpoint of the state space representations the most notable features of the present modified model with combined thermal and strain induced recovery are

1. A finite, elliptical elastic zone that encloses the origin and whose shape is rationalized and suggested by Onat in his extensive discussions on state space [3,19]

2. In creep, the inclusion of strain-induced recovery with an appropriate selection of β allows for the occurrence of steady state creep outside the elastic zone, even without thermal recovery.

3. In relaxation, at low temperatures ($\mathcal{R} = 0$), the present form of the strain induced recovery term results in an asymptotic stress value greater than κ_o that is reached within a shorter time interval. (Note, Robinson's original model, with thermal recovery only, will always saturate to a value equal to κ_o, given sufficient time.)

5.2 Uniaxial Tensile and Cyclic Response

Figures 10 and 11 show the predicted tensile response of the present modified model if we assume no strain recovery and three different rates of loading (i.e., $\overset{\circ}{e}$= 0.001, 0.01 and 0.1/ hr.) for a low homologous temperature (*i.e.*, $\mathcal{R} = 0$; see Fig. 10) and a high homologous temperature (*i.e.*, $\mathcal{R} = 10.535$; see Fig. 11). Notice that at a high homologous temperature the tensile response flattens and gives the appearance of perfect plasticity, whereas at room temperature the response continues to harden within the range of stress investigated. Also, as the rate of loading increases so too does the apparent elastic stress range.

Introducing strain recovery (*i.e.*, $\beta \neq 0$) and maintaining $\mathcal{R} = 0$ (*e.g.*, room temperature) causes the response once again to flatten or saturate to a given level of applied stress (see Fig. 12). This clearly illustrates the proposed modified model's tremendous flexibility in modeling the tensile response over a wide temperature range. Note that the "knee" of the stress-strain curve is much smoother when strain-induced recovery is present (cf. Figs. 11 and 12). Almost identical stress-strain histories are predicted, except for the slightly lowered asymptotic stress level, when both strain and thermal recovery mechanisms are assumed to be active (see Fig. 13); as compared to the case when only strain-induced recovery (Fig. 12) is active. However, comparing the case in which only thermal recovery mechanisms

are active (Fig. 11) to that in which there is both thermal and strain-induced recovery (see Fig. 13), we see a significant drop in saturated stress levels.

Finally, Fig. 14 demonstrates the cyclic behavior of the model if thermal recovery and varying levels of strain-induced recovery (*i.e.*, $\beta = 0,\ 0.5,\ 1.0$) are assumed. Clearly, as the contribution of strain recovery is increased, the maximum attainable stress level is reduced. This is consistent with the monotonic tensile response predicted earlier.

5.3 Multiaxial Tension-Torsion Response

Returning to the multiaxial statement of the proposed modified model given in equations (53) to (63) and assuming that the strain-induced recovery term is zero (*i.e.*, $\beta = 0$), one can quickly conclude that the only difference between the present modified model and that put forth previously [4,14] is the presence of the compliance operator ($Q1_{ijkl}$). The question now becomes whether this operator will have a significant impact on the stress-strain response under multiaxial load histories (recall that the uniaxial response is unaffected by the presence of this compliance operator). To this end, we will examine the effect of this operator under specialized multiaxial load cases, the first one consisting of a proportional tension-torsion history and the second, a nonproportional tension-torsion history (see schematic in Fig. 15). In both cases, stresses will be applied until a specified $\hat{J}_2$ value is reached and then that stress state will be held fixed for a given length of time.

Considering a proportional load path (*i.e.*, $\hat{\tau} = \lambda\hat{\sigma}$) one can show both analytically and numerically that an identical strain response will be generated for both Robinson's model [4] (i.e., eq. (36) with the second term discarded) and the present modified model (Fig. 16). Figure 16 shows the magnitude of inelastic strain (as defined by eqs. (26) and (54)) as a function of nondimensional time Υ for both proportional and nonproportional histories. Note that both Robinson's model and the current modified model give different nonproportional responses, in that the model put forth by Robinson predicts a higher accumulation of inelastic strain than does the modified form. This difference is expected, as indicated by examination of equation (57). Furthermore, as one might expect, the nonproportional response of the two models is initially identical, diverging only when a significant amount of internal deviatoric stress is accumulated with respect to the product $\hat{a}_{ij}\hat{a}_{kl}$. This point is reached at approximately $\Upsilon = 0.00075$ or $t = 2.11$ hours.

At $\Upsilon = 0.001$, both $\hat{\sigma}$ and $\hat{\tau}$ are now constant, and we see that both models predict less accumulation of strain than does the proportional case. If, however, the magnitude of the target $\hat{J}_2$ is doubled from 7.2 to 14.4 (cf. Figs. 16 and 17) then Robinson's model predicts a greater accumulation in inelastic strain during loadup then does the proportional case, whereas the modified form still predicts less than that of the proportional case. Also, as the load level increases so too does the difference between the predicted responses of the two models. For example, at the onset of the constant stress field of $\hat{J}_2 = 7.2$ at $\Upsilon = 0.001$ in Fig. 16 and $\hat{J}_2 = 14.4$ at $\Upsilon = 0.002$ in Fig. 17, the difference in accumulated inelastic strain , $\|\epsilon^I_{ij}\|$, is 0.0008 and 0.011, respectively.

To further illustrate the effect of the compliance operator on the evolution of internal state, in Fig. 18 we show the individual internal deviatoric stress components as a function of nondimensional time for Robinson's model and the present modified form given by equation (55). Note that since $\hat{R} = 0$ and both models are subjected to the same nonproportional history, the difference in internal state can be attributed only to the effect of the compliance operator $Q1_{ijkl}$. From Fig. 18 it is clear that the internal tensile stress of Robinson's model evolves while the torsional component remains unaffected, whereas in the present modified model the internal torsional stress component decreases until the external torsional stress ($\hat{\tau}$) is applied.

Finally, if strain-induced recovery is included (*i.e.*, $\beta \neq 0$), the above trends remain; however, the rate of accumulation of inelastic strain, in both proportional and nonproportional loading histories, is significantly increased (cf. Figs. 16 and 19) because of the material's internal softening due to the mechanical recovery mechanisms.

If we consider the interaction of β and the compliance operator $Q1_{ijkl}$ relative to the nonlinear hard-

ening response, two observations are in order. First, in the uniaxial case either one of these mechanisms can easily be fit to reproduce the nonlinear tensile response. On the other hand, for multiaxial load applications, a unique feature for nonproportionality or path dependency is gained by the inclusion of an internal-state-dependent compliance operator Q.

6 Conclusions

A complete multiaxial potential based viscoplastic model has been presented. It contains in general, three internal state variables (two scalars and one tensor) and both thermal and strain-induced recovery mechanisms. The two scalar internal state variables are associated with dislocation density and are defined as the drag and yield stress. The tensorial variable known as the internal (or back) stress is a second order, traceless, symmetric tensor and is associated with dislocation motion. By merely modifying the definition of the driving threshold function F, this general model was shown to emulate individually or simultaneously, three distinct classes of theories found in the literature. These classes are (1) theories without a yield surface, (2) theories with a threshold surface yet no evolving drag stress, and (3) theories with a threshold surface but with both the drag and yield stress taken to be proportional.

The remainder of the study was dedicated to the assessment of a single tensorial internal state variable (internal stress) model, with the idea of examining the impact of including strain-induced recovery ***and/or*** the compliance operator. A parametric study of a nondimensional multiaxial form examined the model over a wide range of material properties. The important conclusions of that parametric study are listed here:

- In modeling the stress-strain and creep response of metals in the low homologous temperature range, the inclusion of strain-induced recovery provided needed flexibility without adversely affecting the high homologous response.
- Inclusion of strain-induced recovery affected the stress level at which steady state creep occurred for a given internal stress level, the limit stress under both monotonic and cyclic loading, the saturation stress in relaxation, and the elastic domain within the state space.
- Neither uniaxial nor proportional loading histories were affected by the inclusion of the compliance operator; however, with multiaxiality the response due to nonproportional loading paths was significantly influenced.

In light of the forgoing, an important task to consider as future work is the development of an appropriate means of maintaining the nonlinear compliance operator under more general cyclic load conditions without introducing inconsistencies (e.g., internal discontinuities) into the potential framework.

References

[1] Arnold, S.M.; and Saleeb, A.F.: On the Thermodynamic Framework of Generalized Coupled Thermoelastic Viscoplastic - Damage Modeling. NASA TM-105349, 1991

[2] Arnold, S.M.: Effects of State Recovery On Creep Buckling Induced By Thermomechanical Loading. Ph.D. Thesis, University of Akron, Akron, OH, 1987.

[3] Onat, E.T.; and Fardshisheh, F.: Representation of Creep of Metals. ORNL TM-4783, 1972.

[4] Robinson, D.N; and Swindeman, R.W.: Unified Creep-Plasticity Constitutive Equations for 2 1/4 Cr-1Mo Steel at Elevated Temperature. ORNL TM-8444, 1982.

[5] Robinson, D.N.; and Duffy, S.F.: Continuum Deformation Theory for High Temperature Metallic Composites. J. Eng. Mech., vol. 16., no. 4, 1990, pp. 832-844.

[6] Bodner, S. R.: Further Development of a Viscoplastic Constitutive Model for High Temperature Applications. High Temperature Constitutive Modeling — Theory and Applications, A.F. Freed, and K.P. Walker, eds., ASME, New York, 1991, pp. 175-184.

[7] Spencer, A.J.M.: Continuum Physics, Vol. 1, A.C. Eringen, ed., Academic Press., London, 1971, p. 240.

[8] Miller, A.: An Inelastic Constitutive Model for Monotonic, Cyclic, and Creep Deformations: Part I — Equations Development and Analytical Procedures. J. Eng. Mater. Technol., vol. 98, 1976, pp. 97 - 105.

[9] Walker, K.P.: Research and Development Program for Nonlinear Structural Modeling with Advanced time and Temperature Dependent Constitutive Relationship. NASA CR-16533, 1981.

[10] Krempl, E.; McMahon, J.J.; Yao, D.: Viscoplasticity based on Overstress with a Differential Growth Law for the Equilibrium Stress. Mech. Mater., vol. 5, 1986, pp. 35-48.

[11] Chaboche, J.L.: Viscoplastic Constitutive Equations for the Description of Cyclic and Anisotropic Behavior of Metals. Bull. Acad. Pol.Sci., Ser.Sci. Techol., vol. 25, 1977, pp. 33-39.

[12] Freed, A.D.; and Walker, K.P.: A Viscoplastic Model with Application to LiF-22% CaF_2 Hypereutectic Salt. NASA TM-103181, 1990.

[13] Perzyna, P.: On the Constitutive Equations for Work-Hardening and Rate Sensitive Plastic Materials," Bull. Acad. Pol. Sci., Ser. Sci. Techol., vol. 12, 1964, pp. 199-206.

[14] Robinson, D.N.: A Unified Creep -Plasticity Model for Structural Metals at High Temperature. ORNL TM-5969, 1978.

[15] Lemaitre, J.; and Chaboche, J.L.: Mechanics of Solid Materials., Cambridge University. Press, New York, 1990.

[16] Miller, A.K., ed.: Unified Constitutive Equations for Plastic Deformation and Creep of Engineering Alloys. Elsevier Applied Science, New York, 1987.

[17] Freed, A.D.; Chaboche, J.L.; and Walker, K.P.: A Viscoplastic Theory with Thermodynamic Considerations. Acta Mech, vol. 90, 1991, pp. 155-174.

[18] Prager, W.: Introduction to Mechanics of Continua. Ginn and Co., Boston, MA, 1961.

[19] Onat, E.T.; and Fardshisheh F.: Representation of Creep, Rate Sensitivity and Plasticity. SIAM J. Appl. Math., vol. 25, no. 3, 1973, pp. 522-538.

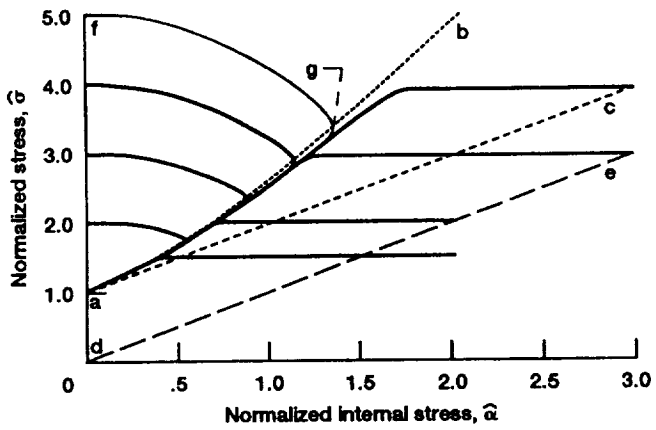

Figure 1.- Calculated $\mathcal{G}$-field (relaxation lines) associated with nondimensional uniaxial simplification, assuming only thermal recovery (*i.e.*, $\beta = 0$; $\mathcal{R} = 10.535$).

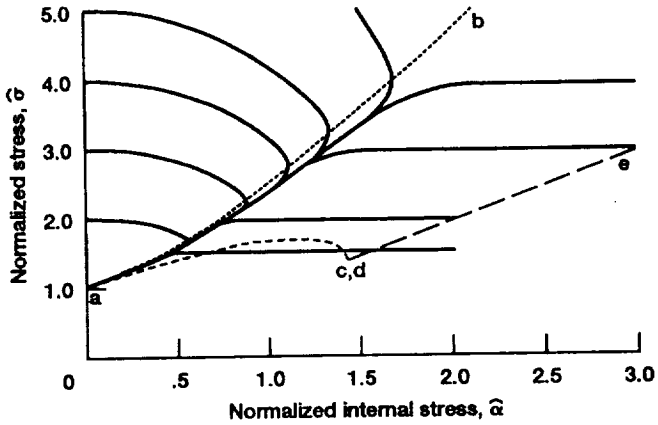

Figure 2.- Calculated $\mathcal{G}$-field (relaxation lines) associated with nondimensional uniaxial simplification, assuming both thermal and dynamic recovery (*i.e.*, $\beta = 0.5$;$\mathcal{R} = 10.535$).

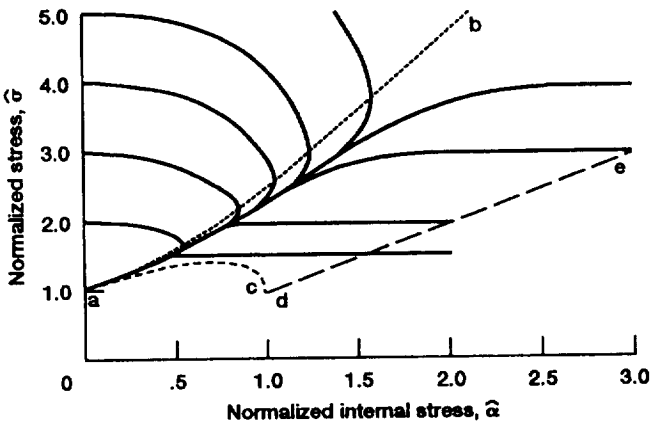

Figure 3.- Calculated $\mathcal{G}$-field (relaxation lines) associated with the non-dimensional uniaxial simplification, assuming both thermal and dynamic recovery (*i.e.*, $\beta = 1.0$; $\mathcal{R} = 10.535$).

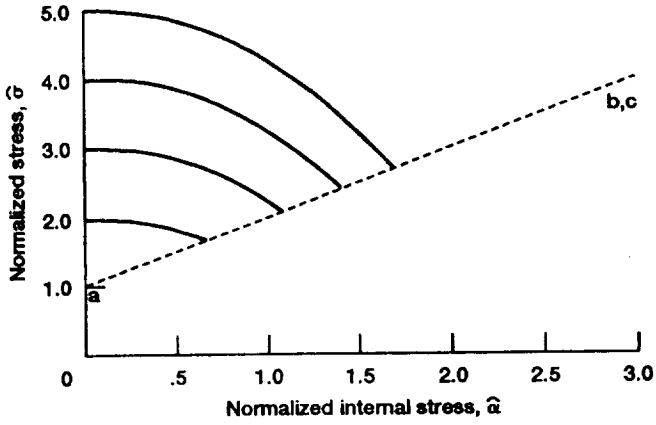

Figure 4.- Calculated $\mathcal{G}$-field (relaxation lines) associated with nondimensional uniaxial simplification, assuming no recovery mechanisms (*i.e.*, $\beta = 0$; $\mathcal{R} = 0$).

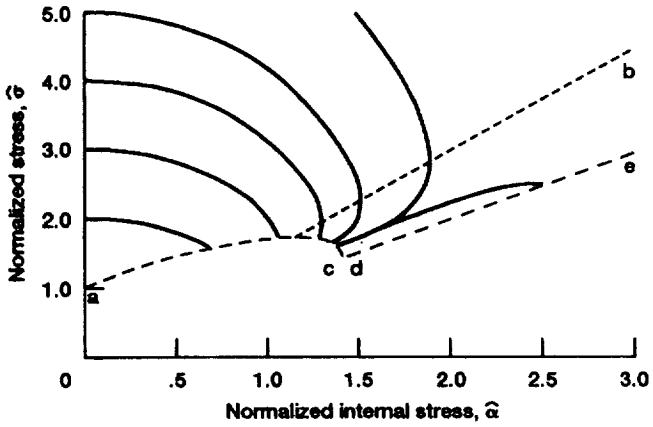

Figure 5.- Calculated $\mathcal{G}$-field (relaxation lines) associated with nondimensional uniaxial simplification, assuming only dynamic recovery (*i.e.*, $\beta = 0.5$; $\mathcal{R} = 0$).

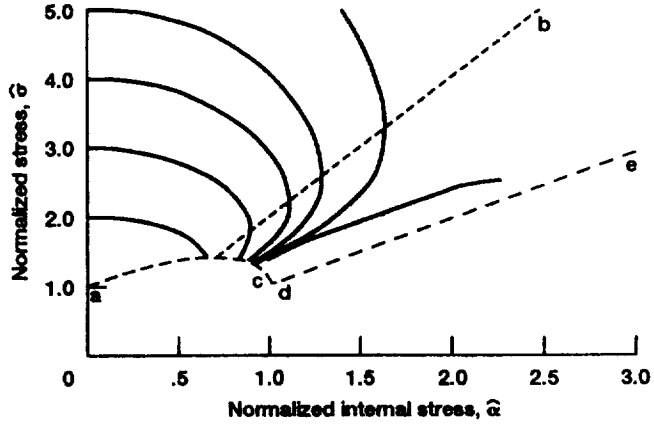

Figure 6.- Calculated $\mathcal{G}$-field (relaxation lines) associated with nondimensional uniaxial simplification, assuming only dynamic recovery (*i.e.*, $\beta = 1.0$; $\mathcal{R} = 0$).

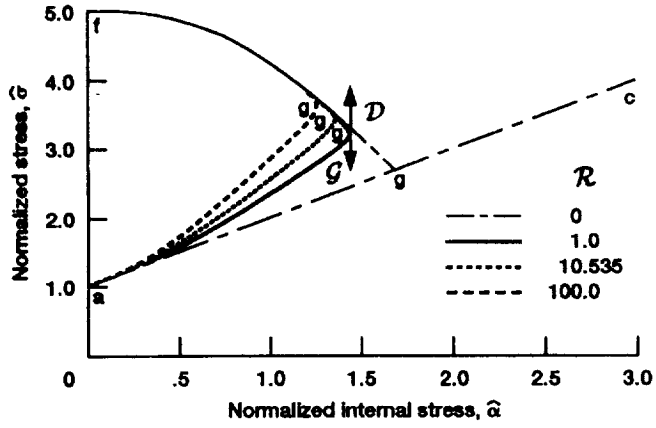

Figure 7.- Effect on relaxation trajectory of varying the amount of thermal recovery (*i.e.*, $\mathcal{R} = 0, 1., 10.535, 100.$) in the absence of any dynamic recovery (*i.e.*, $\beta = 0.$).

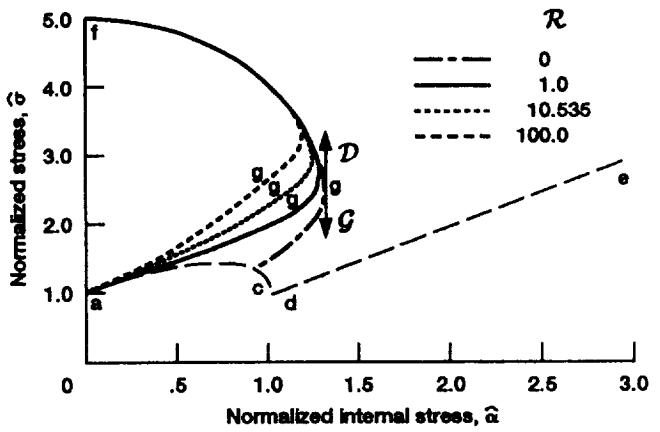

Figure 8.- Effect on relaxation trajectory of varying the amount of thermal recovery (*i.e.*, $\mathcal{R} = 0, 1., 10.535, 100.$) in the presence of dynamic recovery (*i.e.*, $\beta = 1.0$).

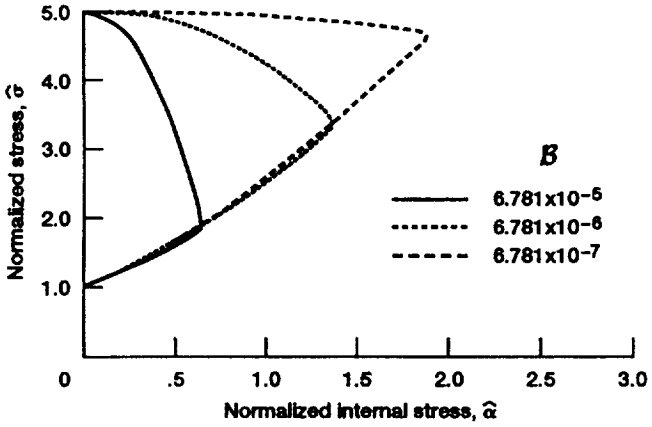

Figure 9.- Effect on relaxation trajectory of varying the amount of viscous-to-plastic dissipation (*i.e.*, $\mathcal{B} = 6.781\text{x}10^{-7}$, $\text{x}10^{-6}$, $\text{x}10^{-5}$) in the presence of thermal recovery only ($\beta = 0$; $\mathcal{R} = 10.535$).

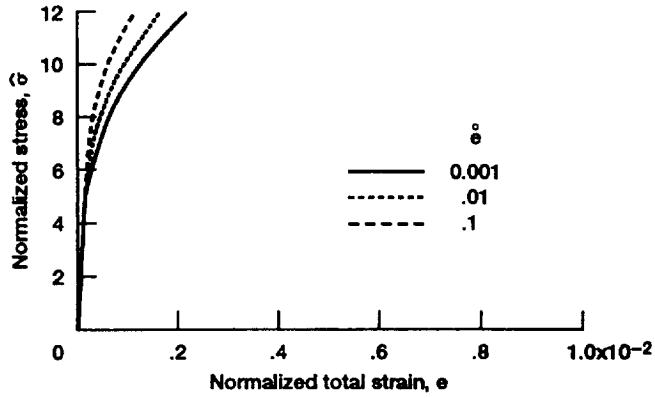

Figure 10.- Effect of strain rate on uniaxial tensile response, assuming no recovery mechanisms present ($\beta = 0$; $\mathcal{R} = 0$).

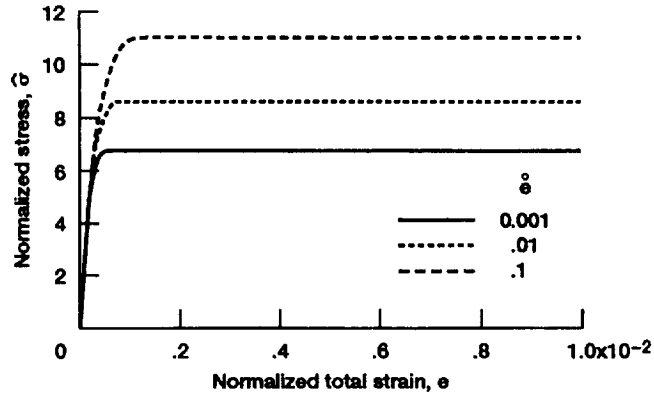

Figure 11.- Effect of strain rate on uniaxial tensile response, assuming only thermal recovery ($\beta = 0$; $\mathcal{R} = 10.535$).

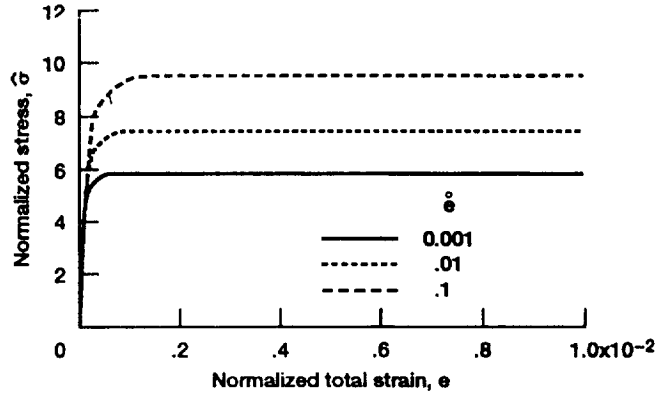

Figure 12.- Effect of strain rate on uniaxial tensile response, assuming only dynamic recovery ($\beta = 1.0$; $\mathcal{R} = 0$).

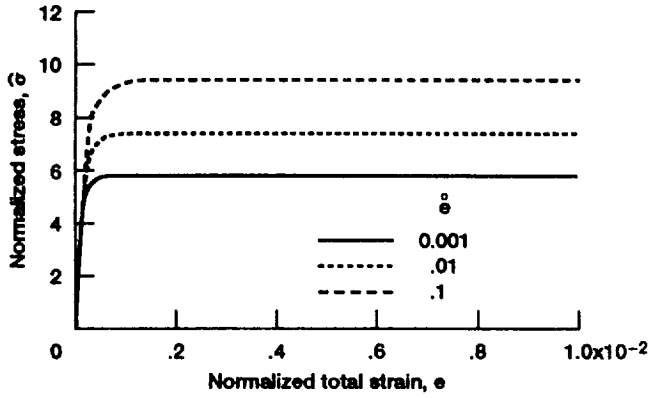

Figure 13.- Effect of strain rate on uniaxial tensile response, assuming both thermal and dynamic recovery ($\beta = 1.0$; $\mathcal{R} = 10.535$).

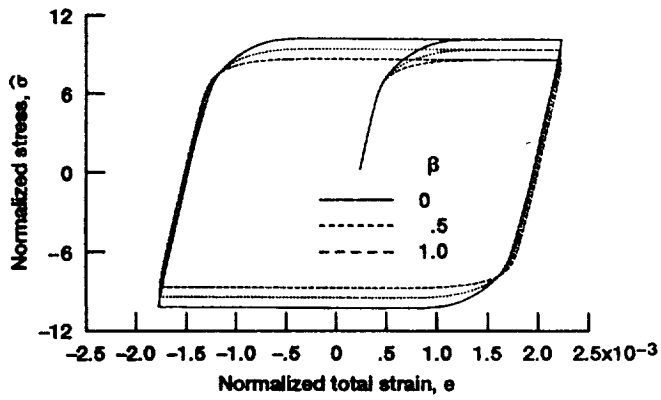

Figure 14.- Uniaxial cyclic response, assuming thermal recovery along with varying levels of dynamic recovery ($\beta = 0$, 0.5, and 1.0).

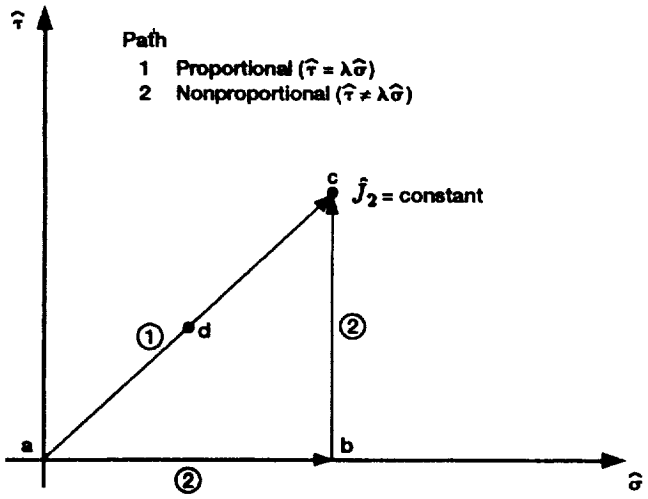

Figure 15.- Schematic of tension - torsion proportional and nonproportional load paths, applicable for both $\hat{J}_2 = 7.2$ and 14.4.

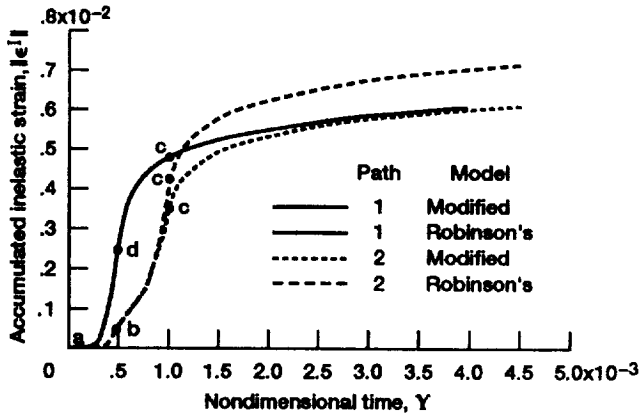

Figure 16.- Magnitude of inelastic strain versus nondimensional time for both proportional and non-proportional loading paths (see fig. 15) with target $\hat{J}_2$ value of 7.2, assuming no recovery mechanisms ($\beta = 0$; $\mathcal{R} = 0$; $\mathcal{B} = 6.781\text{x}10^{-5}$).

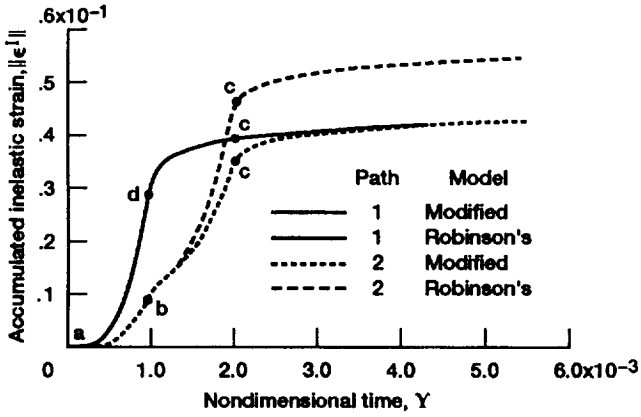

Figure 17.- Magnitude of inelastic strain versus nondimensional time for both proportional and nonproportional loading paths (see fig. 15) with target $\hat{J}_2$ value of 14.4, assuming no recovery mechanisms ($\beta = 0; \mathcal{R} = 0; \mathcal{B} = 6.781\text{x}10^{-5}$).

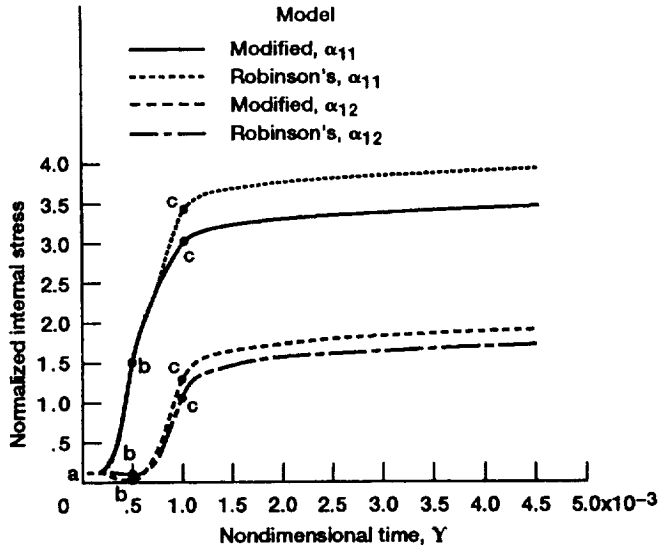

Figure 18.- Normalized internal state (both normal and shear) versus nondimensional time for both proportional and nonproportional loading paths (see fig. 15) with target $\hat{J}_2$ value of 7.2, assuming no recovery mechanisms ($\beta = 0; \mathcal{R} = 0; \mathcal{B} = 6.781\text{x}10^{-5}$).

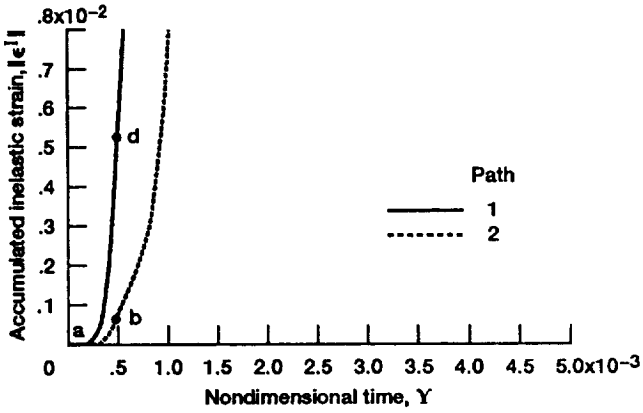

Figure 19.- Magnitude of inelastic strain versus nondimensional time for both proportional and nonproportional loading paths (see fig. 15) with target $\hat{J}_2$ value of 7.2, but assuming dynamic recovery only ($\beta = 0.5$).

REPORT DOCUMENTATION PAGE

Form Approved
OMB No. 0704-0188

1. AGENCY USE ONLY (Leave blank)	2. REPORT DATE	3. REPORT TYPE AND DATES COVERED
	March 1993	Technical Memorandum

4. TITLE AND SUBTITLE

A Modeling Investigation of Thermal and Strain Induced Recovery and Nonlinear Hardening in Potential Based Viscoplasticity

5. FUNDING NUMBERS

WU-510-01-50

6. AUTHOR(S)

S.M. Arnold, A.F. Saleeb, and T.E. Wilt

7. PERFORMING ORGANIZATION NAME(S) AND ADDRESS(ES)

National Aeronautics and Space Administration
Lewis Research Center
Cleveland, Ohio 44135-3191

8. PERFORMING ORGANIZATION REPORT NUMBER

E-7786

9. SPONSORING/MONITORING AGENCY NAME(S) AND ADDRESS(ES)

National Aeronautics and Space Administration
Washington, D.C. 20546-0001

10. SPONSORING/MONITORING AGENCY REPORT NUMBER

NASA TM-106122

11. SUPPLEMENTARY NOTES

S.M. Arnold, NASA Lewis Research Center; A.F. Saleeb, Department of Civil Engineering, University of Akron, Akron, Ohio 44325; and T.E. Wilt, NASA Resident Research Associate, University of Toledo, Toledo, Ohio 43606. Responsible person, S.M. Arnold, (216) 433-3334.

12a. DISTRIBUTION/AVAILABILITY STATEMENT

Unclassified - Unlimited
Subject Category 49

12b. DISTRIBUTION CODE

13. ABSTRACT ***(Maximum 200 words)***

Specific forms for both the Gibb's and the complementary dissipation potentials were chosen such that a complete potential based multiaxial, isothermal, viscoplastic model was obtained. This model in general possesses three internal state variables (two scalars associated with dislocation density and one tensor associated with dislocation motion) both thermal and dynamic recovery mechanisms, and nonlinear kinematic hardening. This general model, although possessing associated flow and evolutionary laws, is shown to emulate three distinct classes of theories found in the literature, by modification of the driving threshold function F. A parametric study was performed on a specialized nondimensional multiaxial form containing only a single tensorial internal state variable (i.e., internal stress). The study was conducted with the idea of examining the impact of including a strain-induced recovery mechanism and the *compliance operator*, derived from the Gibb's potential, on the uniaxial and multiaxial response. One important finding was that inclusion of strain recovery provided the needed flexibility in modeling stress-strain and creep response of metals at low homologous temperatures, without adversely affecting the high temperature response. Furthermore, for nonproportional loading paths, the inclusion of the *compliance operator* had a significant influence on the multiaxial response, but had no influence on either uniaxial or proportional load histories.

14. SUBJECT TERMS

Viscoplasticity; Thermodynamics; Constitutive equations; Nonlinear; Kinematic hardening; Multiaxial; High temperature

15. NUMBER OF PAGES

22

16. PRICE CODE

A03

17. SECURITY CLASSIFICATION OF REPORT	18. SECURITY CLASSIFICATION OF THIS PAGE	19. SECURITY CLASSIFICATION OF ABSTRACT	20. LIMITATION OF ABSTRACT
Unclassified	Unclassified	Unclassified	

National Aeronautics and
Space Administration

Lewis Research Center
Cleveland, Ohio 44135